

# We are IntechOpen, the world's leading publisher of Open Access books Built by scientists, for scientists

6,900

Open access books available

186,000

International authors and editors

200M

Downloads

Our authors are among the

154

Countries delivered to

TOP 1%

most cited scientists

12.2%

Contributors from top 500 universities



WEB OF SCIENCE™

Selection of our books indexed in the Book Citation Index  
in Web of Science™ Core Collection (BKCI)

Interested in publishing with us?  
Contact [book.department@intechopen.com](mailto:book.department@intechopen.com)

Numbers displayed above are based on latest data collected.  
For more information visit [www.intechopen.com](http://www.intechopen.com)



# Bi-Functionalized Hybrid Materials as Novel Adsorbents for Heavy Metal Removal from Aqueous Solution: Batch and Fixed-Bed Techniques

*Yasser Hannachi, Afifa Hafidh and Salwa Ayed*

## Abstract

In this study, two new mesoporous hybrid gels were synthesized. The structural order, morphology, and textural properties of the prepared hybrid materials have been studied by  $^{13}\text{C}$  CP MAS NMR, SEM, FTIR, and nitrogen adsorption-desorption analysis. The application for the heavy metal uptake from aqueous solution using the as-synthesized hybrid materials as an adsorbent is explored. Operating parameters influencing the adsorption procedure, for instance, solution pH, contact time, and temperature are contemplated. In order to gain an insight into the adsorption mechanism and reveal the rate-controlling steps, three models pseudo-first-order, pseudo-second-order, and intra-particle diffusion have been studied to fit. Langmuir, Freundlich, and Dubinin-Radushkevich (D-R) models are assigned to portray the adsorption isotherms. Besides, the feasibility of the synthesized adsorbents for a continuous process in fixed-bed column was investigated. Prior tests produced on electroplating effluents reveal that the as-prepared xerogel could be strongly used for the heavy metal uptake from real wastewater.

**Keywords:** xerogels, adsorption, kinetic, fixed-bed studies, selectivity, reusability

## 1. Introduction

The prompt industrial development and ongoing urbanization have induced growing problems relevant to waste output. Wastes are the generator of hazardous substances which migrate unimpeded through the ecosystem posing severe jeopardy to living organisms. Heavy metals are deemed as a standout among the most toxic groups of inorganic pollutants. The principal origin sources of these heavy metals are usually from electroplating, plastic manufacturing, mining, fertilizers, etc. [1]. The excessive magnitude of these contaminants in industrial wastewaters will severely devastate the ecosystem and human health via accumulation and spreading in the environment and food chain [2]. Faced with the strict environmental enactment, the treatment of wastewater before being discharged into the environment becomes paramount topics worldwide. Diverse treatment processes, for instance, coagulation, precipitation, ion-exchange, reverse osmosis, and

electrolysis, are applied for the remediation of heavy metal ions from aqueous solutions [3–5]. Notwithstanding, by far, the majority of these procedures are restrained by both ecological and economic constraints. In contrast, adsorption has been qualified to be the most relevant and promising method, on account of its low cost, flexible operation, and reversibility. A wide variety of low-cost adsorbents, for example, agricultural by-products, industrial wastes, and natural mineral materials, were found to have good adsorption capacity [6]. However, these materials possess weak resistance to abrasive forces in column apply and leaching of few organics throughout retention process.

It is well known that the substantial factors affecting the adsorption process are pore size distribution, specific surface areas, and pore surface chemistry. In this endeavor, it is imperative to search materials with enormous porous structures, high specific surface areas, and low density. In the last few decades, ordered mesoporous silica has triggered a growing interest in the field of water treatment, owing to its diverse outstanding properties. These enclose tunable pore-size, high specific surface area, large pore volume, chemical inertness, thermal stability, and the ability to attach a plethora of different functional groups [7–9].

One of the basic techniques applied for fabricating organic-inorganic hybrid materials is the sol-gel method. Tetraalkoxysilanes ( $\text{Si}(\text{OR})_4$ ) like tetraethyl orthosilicate (TEOS) or tetramethyl orthosilicate (TMOS) are widely employed as a precursor for preparing monolithic silica, owing to their hydrophobicity and strong covalent Si-O bonding [10]. It is worthy to state that the as-prepared hybrid materials by the sol-gel route are divided into two classes on account of the interaction type between organic and inorganic components. In class I, organic and inorganic components are strongly attached by covalent or dative covalent bonds, while in the second, these two components are weakly bonded through hydrogen or Van der Waals bonds. Indeed, these materials have generated considerable interest for their potential application in multiple fields such as: adsorption [11], drug delivery systems [12, 13], biosensors [14], nanotechnology, and nanomedicine applications [15, 16] and catalysis [17]. Organic-inorganic hybrid materials displayed high efficiency and outstanding selectivity towards target pollutant than the other silica gels. Nitrogen/thiol and magnetic functionalized mesoporous silica have been at the foreground of these composites. In the same vein, Benhamou et al. have shown that amine functionalized MCM-41 and MCM-48 exhibited a higher adsorption capacity than pristine. They also evinced that both hybrid materials have a higher affinity for Cu(II) and Pb(II) than for Cd(II) and Co(II) in single and mixed cation solutions [18]. Shahbazi and co-workers grafted aminopropyl ( $\text{NH}_2$ ) and melamine-based dendrimer amines (MDA) to SBA-15 mesoporous silica. They observed that  $\text{NH}_2$ -SBA-15 and MDA-SBA-15 were over ten-fold better than the pristine SBA-15 in the adsorption of Pb(II), Cu(II), and Cd(II) [19]. Interestingly, they also showed that in column studies, the adsorption yield was swayed by the flow rate. Apart from the fact that magnetic silica-based materials exhibited excellent adsorption affinity towards heavy metal ions, such adsorbents compared to the nitrogen and thiol designer silicates can be easily removed from aqueous solution after adsorption. In the same context, Wang et al. [20] synthesized an amino-functionalized core-shell magnetic mesoporous SBA-15 silica composite which displayed a high adsorption capacity for Pb(II) ions. This adsorbent can be readily removed and regenerated. Despite the high adsorption capacity and the extra-ordinary selectivity towards target metal, as well as the capacity for simultaneous removal of aqueous pollutants, organic-inorganic hybrid materials are still not applied for a continuous process in a fixed-bed column. Another challenge to overcome is the difficulty in their large-scale production because of the complexity of synthesis methods and the control

of the stability of the developed adsorbents. Therefore, great endeavors are required for the synthesis of hybrid silicate adsorbents which meet the listed challenges.

The main aims of the present study were the following:

Firstly, to synthesize and characterize new functionalized hybrid materials and secondly, to assess their ability to remove Zn (II), Cd(II), and Cu(II) ions from aqueous solution. To achieve these goals, experimental parameters affecting the adsorption such as pH solution and contact time were determined. Kinetic data were expressed by pseudo-first-order, pseudo-second-order, and intra-particle diffusion models. Adsorption equilibrium isotherms were evaluated according to Langmuir, Freundlich, and Dubinin-Radushkevich (D-R) models. In addition, the thermodynamic parameters, selectivity, and the reusability have been determined and extensively discussed. To the best of our knowledge, there are scant studies dealing with the applicability of silica hybrid materials for a continuous process in a fixed-bed column. Herein, we have successfully proven the feasibility of the synthesized adsorbents for large volumes of discharges.

## 2. Materials and methods

### 2.1 Chemical reagents

All reagents were of analytical grade and used as received without further purification. Hydrophobic tetraethyl orthosilicate (TEOS, 99%) was utilized as a silica precursor, while ethanol was a bridging medium.  $\text{Cd}(\text{NO}_3)_2 \cdot 4\text{H}_2\text{O}$ ,  $\text{Cu}(\text{NO}_3)_2 \cdot 3\text{H}_2\text{O}$ , and  $\text{Zn}(\text{NO}_3)_2 \cdot 6\text{H}_2\text{O}$  were employed as metal sources for batch and column adsorption experiments. These reagents were supplied by Sigma-Aldrich, USA. The organic precursors 1,3,4-thiadiazole-2,5-diamine and 1,3,4-thiadiazole-2,5-dithiol were prepared according to the literature [21, 22].

### 2.2 Methods

#### 2.2.1 Adsorbent synthesis

Pursuant to our foregoing studies, xerogels were synthesized using the following process [Helali 15 et 16]: 10 ml of deionized water, 20ml of ethanol, and 22.8 mL of TEOS were mixed under vigorous magnetic stirring. To the as-prepared mixture was added a necessary amount of organic precursor ( $10^{-1}$  M, 11.6 g of 1,3,4-thiadiazole-2,5-diamine or 15 g of 1,3,4-thiadiazole-2,5-dithiol). Thereafter, the reactant mixture was stirred for 6 h at 78°C and at the last ripened for 48 h at 100°C; the resulting xerogels were labeled  $\text{M}_1$  and  $\text{M}_2$ , and the synthesis mechanism is represented in **Figure 1**.

#### 2.2.2 Characterization

Xerogel morphology was carried out using a scanning electronic microscope (Cambridge Instruments Stereoscan 120) operating at 15 kV. The textural properties of hybrid materials were determined from the  $\text{N}_2$  adsorption-desorption isotherms recorded at 77 K with a Micrometrics ASAP-2000 volumetric apparatus. The specific surface areas were computed by the multi-point analysis (BET) (Brunauer et al., 1938) in the relative pressure interval of  $0.03 < P/P^\circ < 0.3$ . Howbeit pore size distribution was acquired from the adsorption-desorption branches of the isotherm



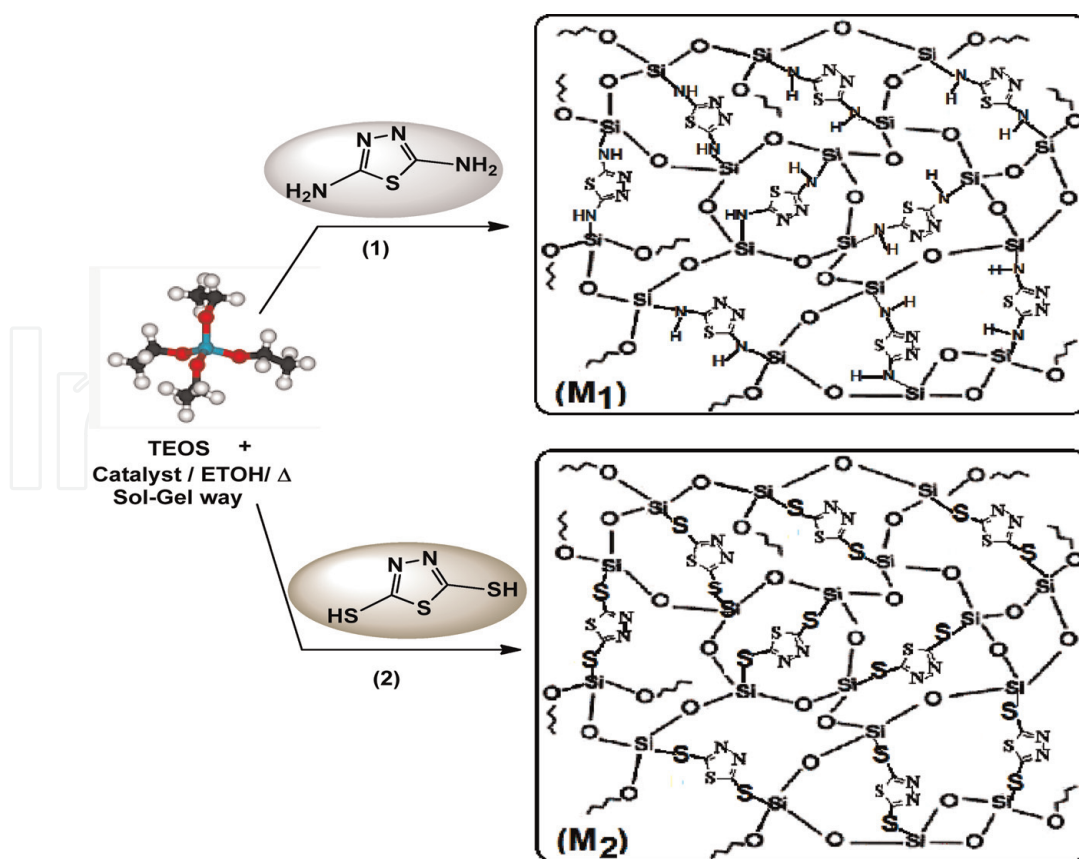


**Figure 1.**  
Synthesis mechanism of hybrid materials  $M_1$  and  $M_2$ .

through the BJH pattern. The total pore volume was evaluated at a relative pressure of  $P/P^* = 0.99$ .

The experimental parameters for the  $^{13}\text{C}$  CP MAS NMR were 9 KHz SPIN rate, 5 s pulse delay. NMR spectroscopy was carried out on an MSL 500 Bruker Spectrometer. FT-IR spectra were collected on 550 Nicolet Magana Spectrometer in KBr pellets in the range of  $4000\text{--}400\text{ cm}^{-1}$ . X-ray photoelectron spectroscopy (XPS) measurement was conducted on a VG ESCALAB MK II spectrometer in the pulse-count mode at a pass energy of 50 eV employing a Mg  $K\alpha$  (1253.6 eV) achromatic X-ray source. In order to evaluate the surface charges, the electro-kinetic potential was performed by Malvern instrument Zeta Nano ZS.

### 2.2.3 Adsorption experiments

Stock solutions were set up by dissolving the required metal mass in 1 L of double-distilled water. Aliquots were prepared by diluting standard stock solution to the desired concentrations ( $5\text{--}400\text{ mg.L}^{-1}$ ). All experiments were done at room temperature in triplicate, and the average values were utilized for further estimation. For every assay, 0.01 g of xerogel was thoroughly blended in conical flasks containing 25 ml of test solution with various metal concentrations at a required pH adjusted prior to the experiment with  $0.1\text{ mol.L}^{-1}$  of  $\text{HNO}_3$  or  $0.1\text{ mol.L}^{-1}$  of NaOH solution. The flasks were shaken for the coveted contact time in an electrically thermostatic reciprocating shaker (Selecta multimatic-55, Spain) at 150 rpm. The contact time for metal ions and the hybrid materials were ranged from 10 to 100 min.

For the adsorption isotherm contemplates, the initial metal concentration was run from  $10\text{ to }400\text{ mg.L}^{-1}$ . After each adsorption procedure, the gathered

examples were centrifuged at 12000 rpm for 20min with the end goal to separate the solid from the liquid phase. The supernatant containing metal ions was evaluated employing an atomic absorption spectrophotometer (SHIMADZU AA-680, Japan). The percent adsorption of metal ion delineated is as follows (Eq. (1)):

$$adsorption\ (%) = \frac{(C_i - C_f)}{C_i} \times 100 \tag{1}$$

where  $C_i$  and  $C_f$  are the initial and final (or equilibrium) adsorbate concentrations, respectively.

2.2.4 Fixed-bed column studies

Dynamic adsorption trial run in the fixed-bed column was conducted in a glass column (3.5 cm length and 1.2 cm diameter), stuffed with 1 g of the xerogel. The metal ion concentration ( $150\text{ mg.L}^{-1}$ ) was pumped in a down flow mode at a flow rate of  $20\text{ mL min}^{-1}$  by using a peristaltic pump (Flowtech India, model NFP01). Samples were gathered at determined time interims, and the residual adsorbate concentration ( $C_e$ ) was measured spectrophotometrically (Eq. (2)). Column exploitation was ceased when the adsorbate concentration attained 95% of its initial concentration. The maximum column capacity ( $q_c$ ) can be reckoned as follows Eq. (3):

$$q_t = A \times Q \times C \times \frac{1}{1000} \tag{2}$$

$$q_e = \frac{q_{total}}{M} \tag{3}$$

where  $q_{total}$  (mg) is the total quantity of adsorbed metal ions, A is the area under breakthrough curve ( $C_e/(C_0)$  versus time, Q ( $\text{mL.min}^{-1}$ ) is the flow rate,  $C_0$  ( $\text{mg.L}^{-1}$ ) is the influent concentration, and M (g) is the mass of adsorbent.

2.2.5 Desorption studies

As a means to examine the regeneration of the synthesized hybrid materials, the metal cation-loaded adsorbents are desorbed with 10 mL of HCl solution (0.5 M) for 60 minutes. Afterwards, the recovered xerogel is flushed with deionized water

Parameters	Values	WHO Standard
pH	2.8	5.5–6.5
Temperature	40	20–30
TSS ( $\text{mg.L}^{-1}$ )	720	20
COD ( $\text{mg.L}^{-1}$ )	371	280
BOD ( $\text{mg.L}^{-1}$ )	90	40
Zn ( $\text{mg.L}^{-1}$ )	100	5
Pb ( $\text{mg.L}^{-1}$ )	10	0.2
Cd ( $\text{mg.L}^{-1}$ )	2	0.1

**Table 1.**  
*Physicochemical characterization of electroplating wastewaters.*

and parched in the air for the forthcoming experiment. Successive sorption-desorption cycles are rehearsed 10 times to build up the genuine application and the high stability of the adsorbent.

### 2.2.6 Adsorption test with the electroplating wastewaters

The effluent specimens are gathered from the discharge exits of electroplating plant, Yaroslavl, Russia. The physicochemical parameters of the electroplating effluent are enlisted in **Table 1**.

Samples are stored in plastic bottles and cooled to 20°C; afterward, they are diluted ten times and alkalized with 0.5 mol.L<sup>-1</sup> of NaOH solution, and finally, are filtered through a 0.35 µm membrane filter. All physicochemical features of the effluent are determined by a conventional procedure [23].

## 3. Results and discussion

### 3.1 Characterization of adsorbents

The morphology of xerogel adsorbents was portrayed by SEM, and the images are illustrated in **Figure 2**.

It very well may be obviously observed that all hybrid materials evinced wrinkled surface and irregular shaped particles with pore diameter over 1.5 nm, indicating the mesoporous structure. The textural properties of the synthesized materials, including specific surface area, total mesoporous volume, and average pore diameter were assessed by N<sub>2</sub> adsorption-desorption isotherms and BJH method. Interestingly, all samples recorded typical type IV adsorption-desorption isotherms which is a characteristic pattern of mesoporous composites as stated in IUPAC classification. Moreover, the hysteresis loop is of type H<sub>2</sub> which is usually tied to the ink-bottle pores with bulky orifice of the border inner parts (**Figure 3**).

A clearly defined step is eventuated roughly at P/P° = 0.4 characteristic of the mesopore filling owing to capillary condensation [24]. Evenly, the pore size curve obtained from the isotherm branch showed a tight distribution centered at about 3.5 nm.

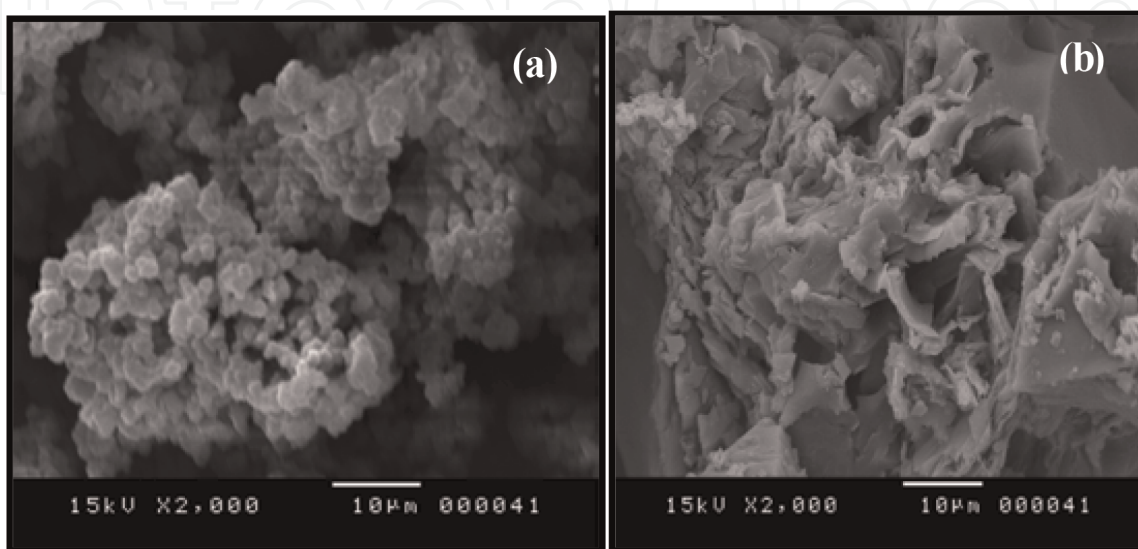


**Figure 2.**  
SEM micrographs of pristine adsorbents: (a)  $M_1$  and (b)  $M_2$ .

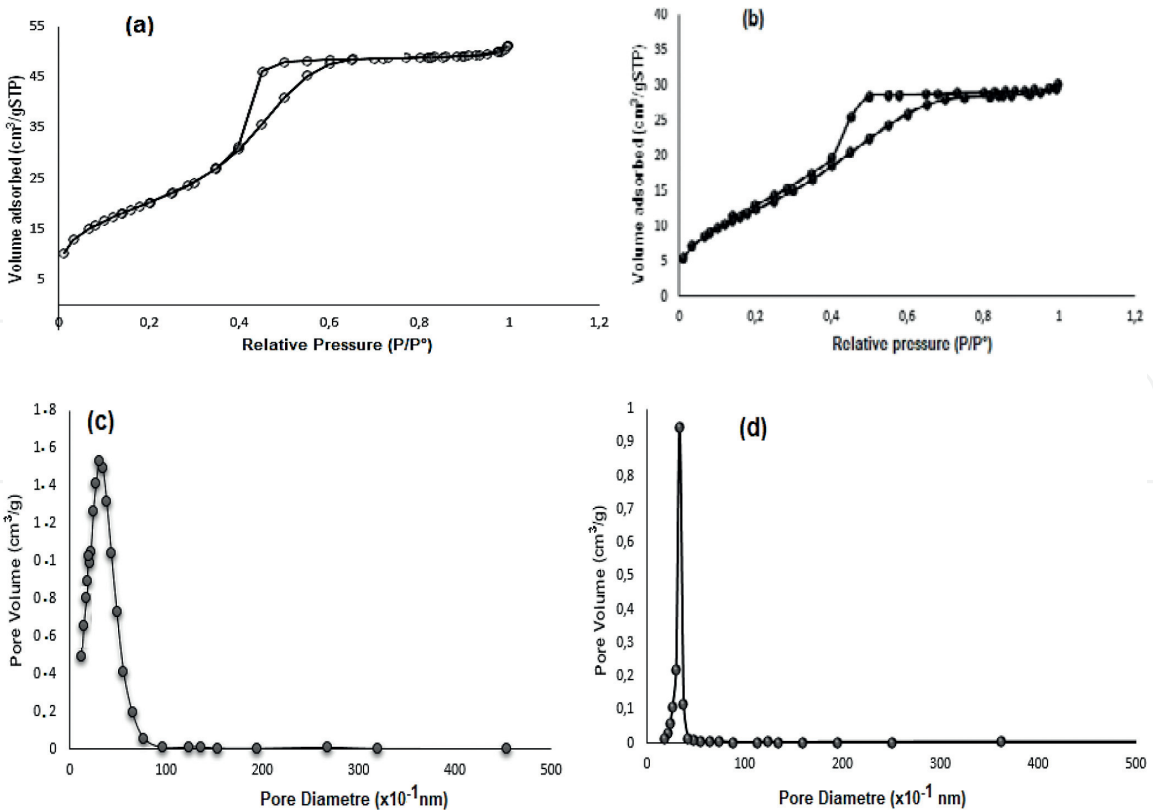


**Figure 3.**  
*N<sub>2</sub> absorption-desorption isotherms of (a) M<sub>1</sub> and (b) M<sub>2</sub> and BJH pore size distribution of (c) M<sub>1</sub> and (d) M<sub>2</sub>.*

Sample	S <sub>BET</sub> (m <sup>2</sup> ·g <sup>-1</sup> )	V <sub>por</sub> (cm <sup>3</sup> ·g <sup>-1</sup> )	d <sub>moy</sub> (Å)
M <sub>1</sub>	290	0.4	34.80
M <sub>2</sub>	310	0.2	20

**Table 2.**  
*BET surface area, pore volume, and average pore size of xerogels M<sub>1</sub> and M<sub>2</sub>.*

Based on data in **Table 2**, all xerogels showed relatively high specific surfaces and pore volumes. More convincing underpins for the successful anchor of organic moieties into the siliceous network emanate from the <sup>13</sup>C CP MAS NMR analysis. The <sup>13</sup>C NMR spectra of the synthesized materials are shown in **Figure 4**. These spectra recorded resonance peaks at 156.3–166.4 ppm (C=N) typical of sp<sup>2</sup> carbon atoms which characterized the cross links of the organic functional groups in the inorganic network, providing the possibility of creating Si-N and Si-S covalent bonds. The peaks at 13–58 ppm were attributed to CH<sub>3</sub>CH<sub>2</sub>O-Si- groups (TEOS). This outcome portrayed the incorporation of the organic bi-functional compounds in the inorganic network, providing the formation of Si-N and Si-S covalent bonds.

So as to confirm the attachment of the organic precursors onto the skeleton of silica species, FT-IR spectroscopy was carried out.

The FT-IR spectra of all samples are depicted in **Figure 5**.

All samples showed a typical band related to Si-O bonds, at 434–440 cm<sup>-1</sup>, bending of O-Si-O at 754–760 cm<sup>-1</sup>, and strong bands at 1061–1134 cm<sup>-1</sup> assigned to the stretching vibration of Si-O-Si groups. Besides, the broad and strong bands detected at 3383–3325 cm<sup>-1</sup> were attributed to the stretching vibration of OH groups which are associated to Si-OH groups ensuing from the TEOS hydrolysis. The signals revealed at 1557–1576 cm<sup>-1</sup> were ascribed to the stretching vibration of C=N groups (heterocyclic part). Another indicative band of the covalent Si-N bond



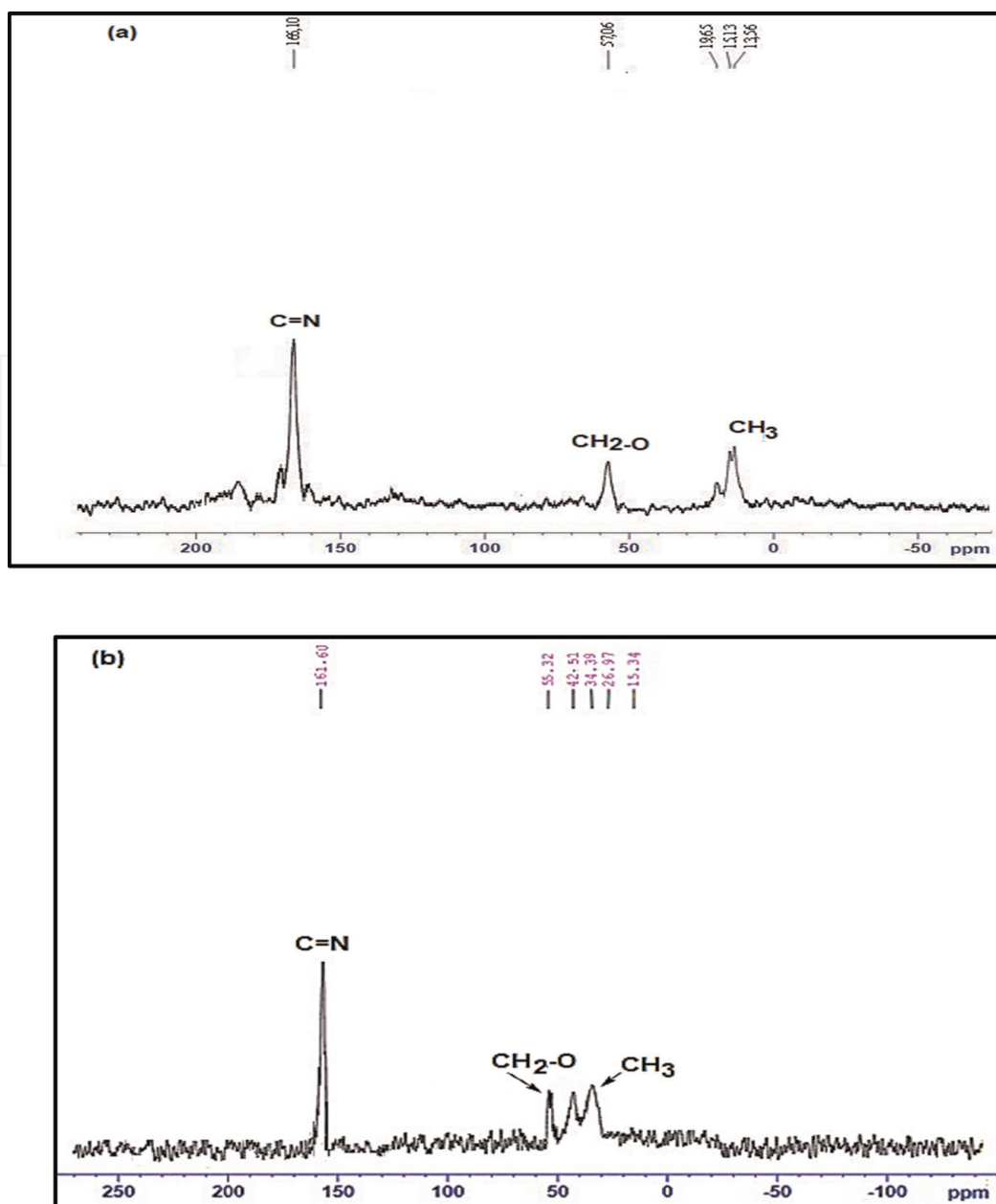


**Figure 4.**  
 $^{13}\text{C}$  NMR CP MAS spectra of  $M_1$  (a) and  $M_2$  (b).

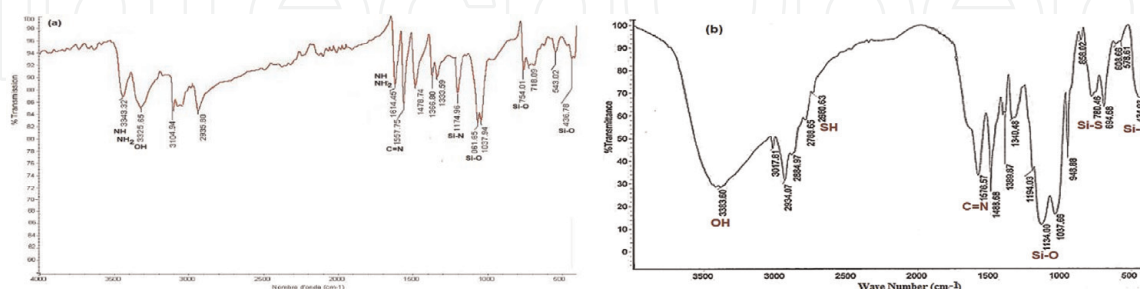


**Figure 5.**  
IR spectra of: (a)  $M_1$  and (b)  $M_2$ .

created between 1,2,4-thiadiazole heterocyclic molecules and the polysiloxane backbone emerged at  $1175\text{ cm}^{-1}$ . The bands located at  $780$  and  $2680\text{ cm}^{-1}$ , attributed to Si-S links and S-H groups, were observed in the  $M_2$  spectrum. In contrast, the signals at  $1614$  and  $3343\text{ cm}^{-1}$  recognize the presence of Si-N links, NH and NH<sub>2</sub> groups, respectively, in  $M_1$  [7].

### 3.2 Effect of pH solution

The pH of the solution is regarded as one of the foremost adsorption factors, since it has a prominent impact on the metal ion solubility, as well as on the adsorbent surface metal binding sites.

The effect of pH on the removal efficiency of heavy metal ions by hybrid materials was assessed inside a scope of 2–10. Zeta potential is the best and reliable method to determine the adsorbent surface charge, which was characterized by point of zero charge (pHpzc). The pH of zero charge (pHZps) of the as-prepared xerogels  $M_1$  and  $M_2$  is recognized to be  $4.6 \pm 0.2$  and  $4.2 \pm 0.2$ , respectively (Figure 6).

As illustrated in Figure 6, when  $pH < pHZps$ , the adsorbent surface charge is positive by virtue of the amino and thiol group protonation. Therefore, electrostatic repulsive force emerges between heavy metal ions and the adsorbent surface, inciting abatement in the adsorption capacity. Be that as it may, at  $pH > pHZps$ , all samples earn a negative surface charge, promoting electrostatic attraction between metal cations and adsorbent and therefore, the absorption efficiency enhancement. It ought to be stressed that beyond pH 5 [25], the uptake yield of heavy metal ions diminishes through the metallic hydroxide precipitation which thwarts the diffusion of the metal ions into the adsorbent active site. Therethrough, the pH at 7 was selected as the ideal incentive in the resulting experiments (Figure 7).

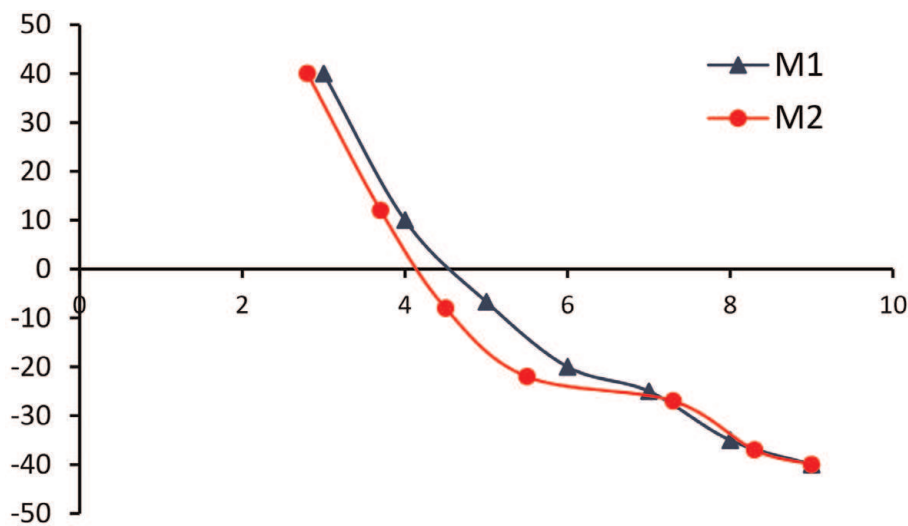


**Figure 6.**  
Zeta potential of xerogels at different pH values.

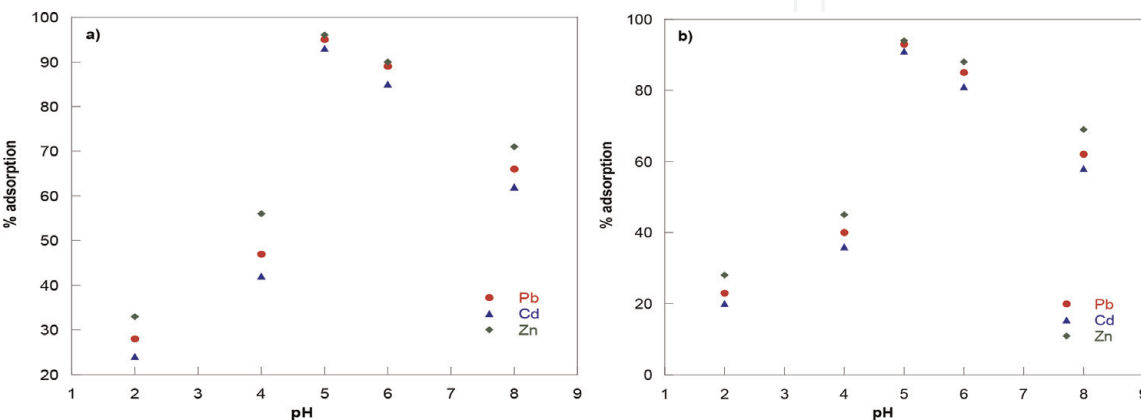


**Figure 7.**  
Effect of pH on adsorption of metal ions onto both xerogels ((a)  $M_1$  and (b)  $M_2$ ) (metal concentration  $20 \text{ mg. L}^{-1}$ ; adsorbent dosage  $0.4 \text{ g.L}^{-1}$ , contact time 1 h).

### 3.3 Adsorption kinetics

The contact time is well recognized as the dwelling time of sorbate uptake at the superficial adsorbent surface. To study the effect of contact time, 0.015 g of hybrid materials was thoroughly mixed in 25 mL of initial metal concentration  $20 \text{ mg.L}^{-1}$  and was shaken at a rotational speed of 150 rpm.

As portrayed in **Figure 8**, the heavy metal adsorption onto the three xerogels rapidly increased in the first 40 min; thereafter, it becomes slower and in the later stage reaches to saturation (equilibrium). Further increase in contact time did not ameliorate the uptake efficiency; this trend may be attributed to the fact that padding of void active sites becomes impossible owing to the electrostatic repulsion between the solute ions of the adsorbent and bulk phases [26]. Thus, 60 min is seen fit to attain equilibrium in ulterior trials.

In order to acquire an insight into the adsorption mechanism and reveal the rate controlling steps, three kinetic models including pseudo-first-order, pseudo-second-order, and intra-particle diffusion were checked.

The adsorption rates were first examined by Lagergren's pseudo-first-order [27] and its linearized integral form is spoken to as follows in Eq. (4):

$$\ln(q_e - q_t) = \ln q_e - k_1 t \quad (4)$$

where  $q_t$  and  $q_e$  ( $\text{mg.g}^{-1}$ ) are the adsorption capacities at equilibrium ( $\text{mg.g}^{-1}$ ) and  $t$  (min), respectively, and  $k_1$  is the rate constant of the equation ( $\text{min}^{-1}$ ). The rate constant,  $k_1$ , equilibrium adsorption capacity,  $q_e$ , and the correlation coefficient  $R^2$ , are determined experimentally by plotting  $\ln(q_e - q_t)$  versus  $t$ . The allied parameters are listed in **Table 1**.

The pseudo-second-equation provided by Ho [28] can be stated by the pursuing equation Eq. (5):

$$\frac{t}{q_t} = \frac{1}{k_2 q_2^2} + \frac{t}{q_2} \quad (5)$$

where  $k_2$  ( $\text{g.mg}^{-1} \text{ min}^{-1}$ ) is the rate constant and  $q_2$  is the amount of adsorption equilibrium capacity ( $\text{mg.g}^{-1}$ ). The values of  $q_e$  and  $k_2$  can be determined graphically from the slope and the intercept of the plot  $t/q_t$  versus  $t$  at different temperatures.

The kinetic parameters gained from pseudo-first-order and pseudo-second-order are introduced in **Table 3**. It is obvious that the theoretical adsorption

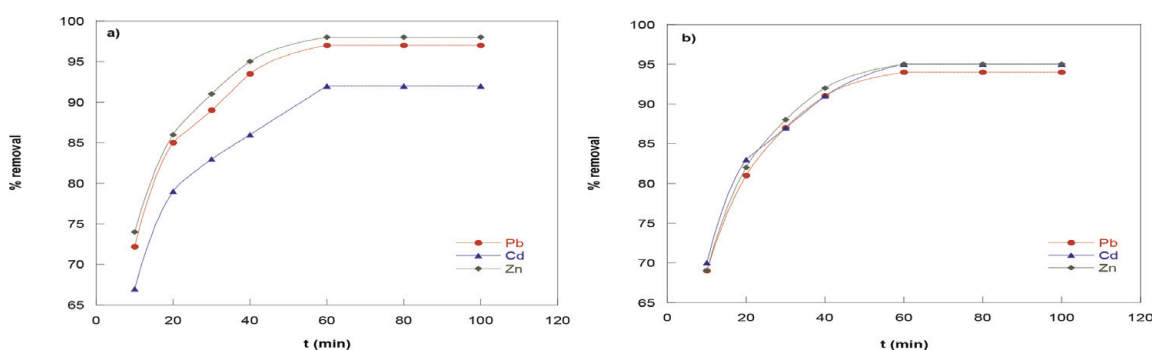


**Figure 8.**

Effect of contact time and temperature on adsorption of metal ions by the two adsorbents (metal concentration:  $20 \text{ mg.L}^{-1}$ ; adsorbent dosage:  $0.4 \text{ g.L}^{-1}$ ; pH: 5): (a)  $M_1$  and (b)  $M_2$ .

capacities ( $(q_{th})$ ) evaluated from the pseudo-second-order equation were very close to experimental ( $q_e$  (ex)) values; besides, the correlation coefficients related to the above-mentioned model were found to be higher than those ascertained from the pseudo-first-order equation. These unequivocally propose that the pseudo-second-order model, as opposed to the pseudo-first-order model, is more suitable to depict the adsorption procedure.

By the by, the aforementioned kinetic models cannot identify the diffusion mechanism and also, the rate controlling step of the adsorption kinetic process. In this regard, it is important to apply the Weber and Morris intra-particle diffusion model. This later assumes that the adsorption process might be controlled either by one of the resulting steps, namely film diffusion, pore diffusion, and adsorption onto the inner sites of adsorbent or a mix of a few stages (multi-step process) [29]. The rate parameter for intra-particle diffusion is displayed as follows Eq. (6):

$$q_t = K_{id}t^{0.5} + C \tag{6}$$

where  $K_{id}$  is the intra-particle rate constant ( $mg.g.min^{0.5}$ ) obtained from the slope of the straight line  $q_t$  versus  $t^{0.5}$  and C is the intercept corresponding to the boundary layer thickness. If the rate of adsorption is controlled only by the intra-particle diffusion, the value of C should be zero ( $C = 0$ ) and the plots of  $q_t$  against  $t^{0.5}$  provide a straight line passing through the origin.

As depicted in **Figure 9**, all the plots show multi-linear uptake revealing three adsorption stages. The first steep-sloped portion corresponds to the transport of

Metal ions	$q_e\text{ exp}$ ( $\text{mg g}^{-1}$ )	Pseudo-first-order kinetic			Pseudo-second-order kinetic		
		$k_1(\text{min}^{-1})$	$q_{e\text{ cal}}(\text{mg}\cdot\text{g}^{-1})$	r	$k_2(\text{g mg}^{-1}\text{ min}^{-1})$	$q_{e\text{ cal}}(\text{mg g}^{-1})$	r
M <sub>1</sub>							
Pb <sup>2+</sup>	285	$5.7.10^{-4}$	178	0.958	$17.3.10^{-4}$	278	0.998
Cd <sup>2+</sup>	234	$2.8.10^{-4}$	167	0.953	$8.02.10^{-4}$	38	0.999
Zn <sup>2°</sup>	410	$7.5.10^{-4}$	249	0.936	$19.9.10^{-4}$	380	0.998
M <sub>2</sub>							
Pb <sup>2+</sup>	261	$4.6.10^{-4}$	185	0,926	$14.8.10^{-4}$	265	0.998
Cd <sup>2+</sup>	214	$2.4.10^{-4}$	150	0,942	$7.3.10^{-4}$	199	0.997
Zn <sup>2+</sup>	360	$6.6.10^{-4}$	210	0,912	$17.8.10^{-4}$	320	0.999

**Table 3.**  
*Pseudo-first-order and pseudo-second-order parameters for the adsorption of Pb (II), Cd (II), and Zn (II) onto two adsorbents at different temperatures.*

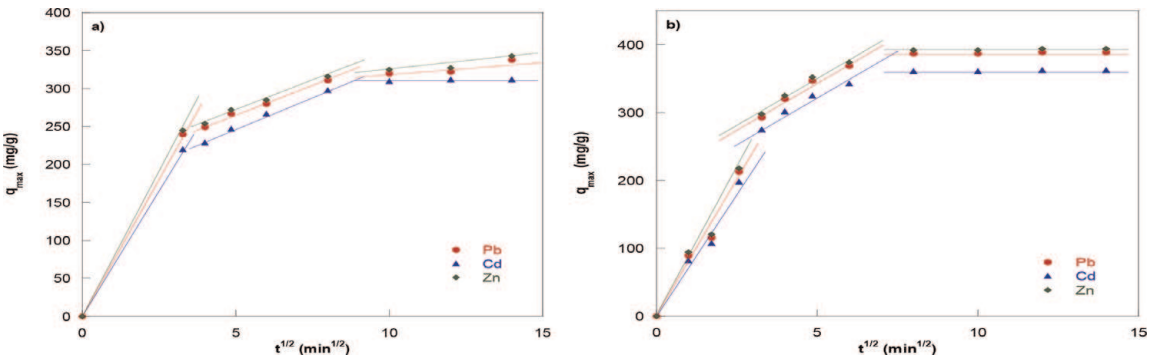


**Figure 9.**  
*Intra-particle diffusion plots model for metal ions adsorption onto (a) M<sub>1</sub> and (b) M<sub>2</sub>.*



Sample	$K'_1 \text{ (mg.g}^{-1}\text{.min}^{-0.5}\text{)}$	$K'_2 \text{ (mg.g}^{-1}\text{.min}^{-0.5}\text{)}$	$K'_3 \text{ (mg.g}^{-1}\text{.min}^{-0.5}\text{)}$
M <sub>1</sub> -Pb	10.252	4.792	2.103
M <sub>2</sub> -Pb	12.348	6.453	3.501
M <sub>1</sub> -Cd	11.457	5.395	3.424
M <sub>2</sub> -Cd	12.567	6.637	3.667
M <sub>1</sub> -Zn	10.684	5.138	2.735
M <sub>2</sub> -Zn	12.729	6.841	3.829

**Table 4.**  
*Intra-particle diffusion adsorption rate constants of metal ions onto the two adsorbents.*

metal ions from bulk solution to the adsorbent external surface via film diffusion. The second stage describes the progressive adsorption step, indicating the diffusion of adsorbate through the pores of xerogel (intra-particle diffusion). The third small-sloped section corresponds to the final equilibrium stage where the intra-particle diffusion commences progressively to slow down because of the quick abatement of metal cation concentrations. Intra-particle diffusion model parameters are enrolled in the **Table 4**.

The boundary layer parameter C was diverse to zero, showing that the intra-particle diffusion ought not to be the sole rate limiting step [30]. Be that as it may, it ought to be accentuated that the rate controlled step was governed by film-diffusion towards the start and afterward followed by intra-particle diffusion.

3.4 Adsorption isotherms

Adsorption isotherm is viewed as a standout amongst the most critical elements for determining the mechanism between adsorbent and adsorbate. In this research, Langmuir, Freundlich, and Dubinin-Radushkevich (D-R) isotherm models were utilized to assess the equilibrium data.

The Langmuir isotherm model expects the formation of monolayer coverage of adsorbate on the external surface of adsorbent and a finite number of equipotential sites [31]. The Langmuir model can take the following linear form Eq. (7):

$$\frac{C_e}{q_e} = \frac{1}{q_{max}K_L} + \frac{C_e}{q_{max}} \tag{7}$$

where  $q_e$  is the amount of metal cations adsorbed by unit weight of adsorbent (mg. g<sup>-1</sup>),  $C_e$  is the equilibrium concentration of adsorbate in the solution (mg. L<sup>-1</sup>),  $q_{max}$  is the maximum adsorption capacity at monolayer coverage (mg.g<sup>-1</sup>), and  $K_L$  is the Langmuir adsorption constant (L.mg<sup>-1</sup>). Linear plots of  $C_e/q_e$  against  $C_e$  were used to determine the value of  $q_{max}$  (mg.g<sup>-1</sup>) and  $K_L$  (L.mg<sup>-1</sup>). The data obtained with the correlation coefficients ( $R^2$ ) are reported in **Table 5**.

The Freundlich isotherm is an experiential equation which presumes various affinities for the binding sites on the surface of the adsorbent accompanied by the interactions between adsorbed molecules. The linear form of the Freundlich adsorption isotherm [32] can be communicated as follows Eq. (8):

$$\log q_e = \log k_f + \frac{1}{n} \log C_e \tag{8}$$

where  $k_f$  is a constant related to the bonding energy and n is a measure of the deviation from linearity and the heterogeneity degree of adsorption sites. The

	Langmuir parameters			Freundlich parameters			D-R parameters		
	$q_m$ (mg.g <sup>-1</sup> )	$K_L$ (L mg <sup>-1</sup> )	$R^2$	$K_F$	1/n	$R^2$	$q_m$ (mol.g <sup>-1</sup> )	$E$ (KJ mol <sup>-1</sup> )	$R^2$
<b>M<sub>1</sub></b>									
Pb <sup>2+</sup>	523	0.07	0.998	75.85	0.38	0.845	3.73.10 <sup>-4</sup>	13.1	0.993
Cd <sup>2+</sup>	507	0.05	0.997	128	0.27	0.871	2.64.10 <sup>-4</sup>	13	0.991
Zn <sup>2+</sup>	578	0.1	0.999	149	0.42	0.832	4.69.10 <sup>-4</sup>	13.63	0.994
<b>M<sub>2</sub></b>									
Pb <sup>2+</sup>	509	0.09	0.997	135	0.27	0.836	4.51.10 <sup>-4</sup>	12.82	0.995
Cd <sup>2+</sup>	493	0.04	0.998	67	0.41	0.883	3.34.10 <sup>-4</sup>	13.33	0.992
Zn <sup>2+</sup>	549	0.09	0.998	140	0.37	0.842	4.57.10 <sup>-4</sup>	13.22	0.993

**Table 5.**  
*Langmuir, Freundlich, and D-R parameters for Pb (II), Cd (II), and Zn (II) adsorption onto mesoporous materials M<sub>1</sub> and M<sub>2</sub>.*

Freundlich equilibrium constants  $k_f$  and 1/n were determined from the slopes and intercepts of the linear plot of  $\log q_e$  versus  $\log C_e$ . The values for Freundlich constants and correlation coefficients ( $R^2$ ) for the adsorption process are also recorded in **Table 5**.

As can be seen, the adsorption capacity is higher for **M<sub>1</sub>** than **M<sub>2</sub>**. This pattern could be related to the specific surface area as well as to the structure of the amino groups which displayed a high chelating ability to heavy metal ions. However, the isotherm parameters, together with the correlation coefficients showed that the Langmuir model gives a good fit to the adsorption isotherm. Additionally, the Freundlich adsorption capacity  $k_f$  is higher for **M<sub>1</sub>** than **M<sub>2</sub>**. The n values which mirror the adsorption intensity also presented the same trend. The acquired values n for both adsorbates model that the adsorption process onto mesoporous material was favorable at considered conditions. However, compared to the  $R^2$  values, with that obtained from the Langmuir model, it can be remarkably noted that the Langmuir isotherm model better fits the equilibrium data.

The Dubinin-Radushkevich (D-R) model is a semi-hypothetical equation which is by and large allied to a sorption induced by a pore padding mechanism. This model gives valuable information on the nature of the adsorption process (chemisorption or physisorption) [33]. The linear presentation of the D-R isotherm equation [34] is granted as Eq. (9):

$$\log q_e = \log q_m - \beta \varepsilon^2 \tag{9}$$

where  $q_e$  is the adsorption capacity (mol.g<sup>-1</sup>),  $q_m$  is the maximum adsorption capacity (mol.g<sup>-1</sup>),  $\beta$  is the activity coefficient which gives an idea about the mean free energy (mol<sup>2</sup>.J<sup>-2</sup>), and  $\varepsilon$  is the Polanyi potential [ $\varepsilon = RTLn\left(1 + \frac{1}{C_e}\right)$ ]. The values of  $q_m$  and  $\beta$ , can be generated from the slope and the intercept of the plot  $\ln q_e$  versus  $\varepsilon^2$ . The adsorption mean free energy ( $E$ , kJ.mol<sup>-1</sup>) can be calculated using Eq. (10):

$$E = \frac{1}{\sqrt{-2\beta}} \tag{10}$$

In addition, the magnitude of  $E$  (kJ.mol<sup>-1</sup>) value provided data about the type of adsorption mechanism, either physical or chemical. The maximum adsorption

capacity  $q_m$ , the adsorption free energy  $E$ , and the coefficients of linearity are computed and spoken to in **Table 5**. As observed from the table, the high correlation coefficients ( $\geq 0.99$ ) propose that the adsorption equilibrium data fitted well the D-R isotherm model. Moreover, the mean adsorption energy values were in the range of 13–14  $\text{kJ}\cdot\text{mol}^{-1}$  for all samples. In perspective of the acquired outcomes, it tends to be reasoned that the adsorption processes of metal ions onto the as-prepared xerogels might be proceeded by chemisorption (binding surface functional groups) [35].

4. Column studies

It is well known that the column trials were conducted to predict the necessary residence time of effluent treatment with a specific flow rate and concentration (**Figure 10**).

It ought to be stressed that the breakthrough curves characterize the dynamic performance of saturated columns; delineated as the ratio of effluent concentration to influent concentration over time. The time where the pollutant concentration in effluent reached 5% is called breakthrough time ( $t_b$ ); however, the time taken for the effluent concentration to attain 95% of initial pollutant concentration is appealed exhaustion time. The Breakthrough curves for metal ion adsorption onto both adsorbents are portrayed in **Figure 6** and their column data are tabulated in **Table 6**.

As portrayed in **Figure 10**, all breakthrough curves exhibited an S-shaped profile; besides, earlier breakthrough and exhaustion times were observed for  $M_2$

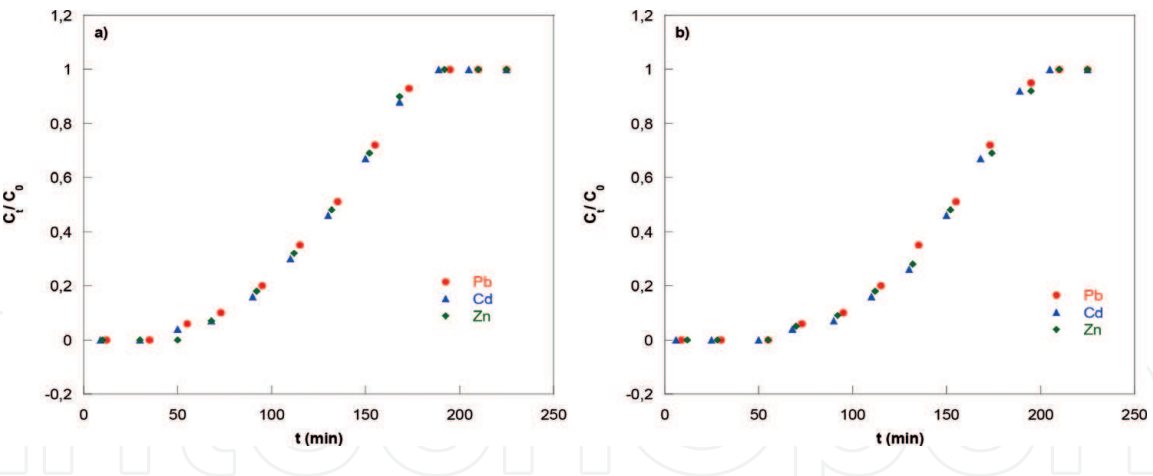


**Figure 10.**  
Breakthrough curves for metal ion adsorption onto mesoporous materials  $M_1$  (b) and  $M_2$  (a).

	Metal	Breakthrough time	Exhaustion time	Breakthrough capacity ( $\text{mg}\cdot\text{g}^{-1}$ )
M1	Zn (II)	45	185	442
	Pb (II)	42	179	410
	Cd (II)	40	175	403
M2	Zn (II)	38	175	420
	Pb (II)	36	172	406
	Cd (II)	35	170	394

**Table 6.**  
Column data for metal ion adsorption.

xerogel, while  $M_1$  displayed a longer breakthrough time. It is clear that breakthrough capacities calculated from column studies were lesser than those settled from the batch method. This pattern might be because of the impact of the prolonged residence time of the sorbate as well as the agitation speed which improve the adsorption in the batch technique. It is worthy to state that the grand breakthrough capacity of  $M_1$  is related to its longer breakthrough time.

4.1 Column regeneration

The regeneration ability is an essential factor for metal recovery and the applicability of adsorbents. The metal charged column was regenerated with 0.1 M HCl (40 mL) and then with 0.5 M HNO<sub>3</sub> (20 mL) at a flow rate of 7 mL.min<sup>-1</sup>. Afterwards, each column was washed with 60 mL of hot deionized water and then dried in an oven at 60°C. The adsorption efficiency of the exhausted column was checked five times. The uptake yield decreased from 96%–94% to 90%–88% for  $M_1$  and 93%–91% to 87%–86% for  $M_2$  after five adsorption-desorption cycles (Figure 11). The acquired outcomes uncovered that the as-prepared xerogels could be effortlessly regenerated and continuously used in the metal cation removal process without an obvious decrease in the total adsorption performance.

4.2 Thermodynamic parameters

The mechanism of adsorption can be checked through determining thermodynamic parameters like Gibbs free energy ( $\Delta G^\circ$ ), enthalpy ( $\Delta H^\circ$ ), and entropy ( $\Delta S^\circ$ ). These parameters can be determined from the following equations: Eqs. (11) and (12):

$$\ln K_L = \frac{\Delta S}{R} - \frac{\Delta H}{RT} \text{ (Van't Hoff equation)} \tag{11}$$

$$\Delta G^\circ = -RT \ln K_L \tag{12}$$

where  $K_L$  is the Langmuir constant (L.mol<sup>-1</sup>),  $T$  is the absolute temperature (K), and  $R$  is the gas constant. By plotting  $\ln K_L$  against  $1/T$ , it is possible to determine graphically the value of  $\Delta H^\circ$  from the slope, and the value of  $\Delta S^\circ$  from the intercept (Figure 12). The calculated parameters are given in Table 7.

The values of Gibbs free energy change  $\Delta G^\circ$  were negative at various temperatures indicating that the adsorption of the two pollutants onto the as-synthesized adsorbent was feasible and spontaneous. Notwithstanding, the abatement of  $\Delta G^\circ$  values with temperature could be clarified by a diminishment in the mobility of the metal and the adsorption driving force [36]. The negative value of  $\Delta G^\circ$  affirmed the

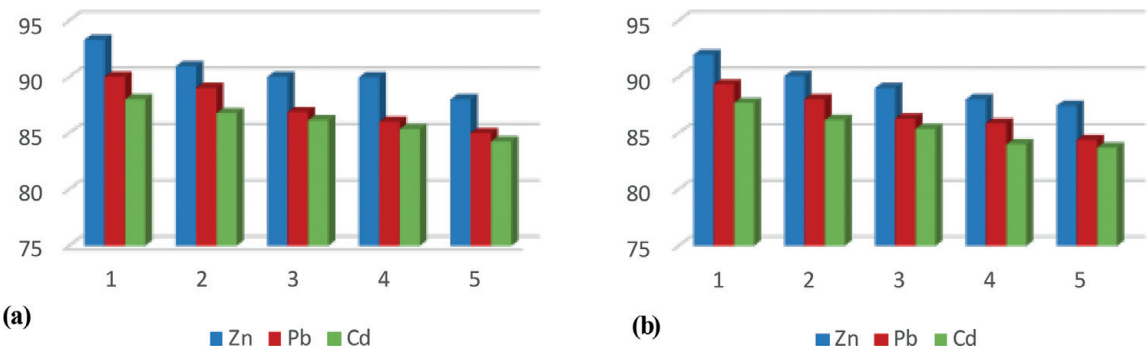
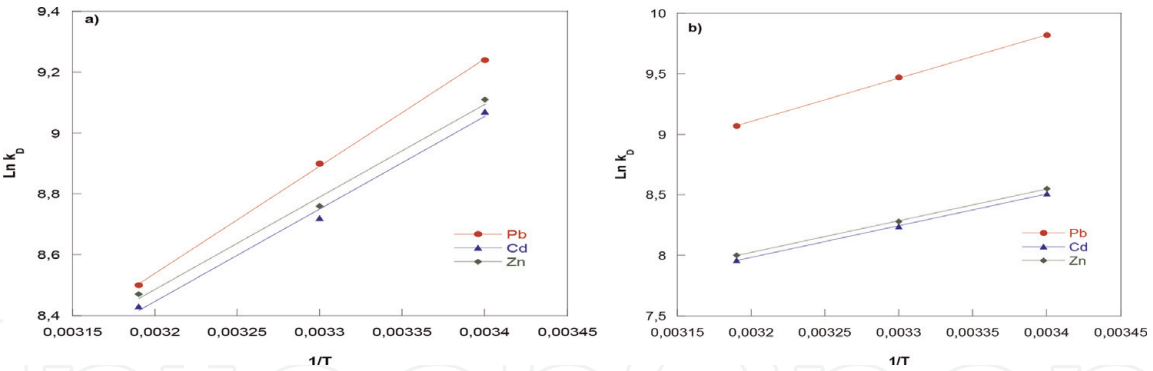


Figure 11. Adsorption-desorption efficiency of xerogels after 5 cycles: (a)  $M_1$  and (b)  $M_2$ .





**Figure 12.**  
Determination of thermodynamic parameters for the adsorption of metal cations onto the two adsorbents: (a)  $M_1$  and (b)  $M_2$ .

Pb (II)	T(K)	$\Delta G^0 (kJ.mol^{-1})$	$\Delta H^0 (kJ.mol^{-1})$	$\Delta S^0 (J.mol^{-1}.K^{-1})$
$M_1$	293	-22.51	-74.67	-162.3
	303	-21.82		
	313	-20.94		
$M_2$	293	-23.92	-62.23	-143.31
	303	-22.89		
	313	-22.19		

Cd(II)	T(K)	$\Delta G^0 (kJ.mol^{-1})$	$\Delta H^0 (kJ.mol^{-1})$	$\Delta S^0 (J.mol^{-1}.K^{-1})$
$M_1$	293	-22.08	-69.08	-157.71
	303	-21.72		
	313	-21.55		
$M_2$	293	-20.72	-59.86	-131.34
	303	-20.53		
	313	-20.39		

Zn(II)	T(K)	$\Delta G^0 (kJ.mol^{-1})$	$\Delta H^0 (kJ.mol^{-1})$	$\Delta S^0 (J.mol^{-1}.K^{-1})$
$M_1$	293	-23.16	-80.12	-172.35
	303	-22.93		
	313	-22.75		
$M_2$	293	-21.87	-66.74	-152.27
	303	-21.64		
	313	-21.41		

**Table 7.**  
Thermodynamic parameters for heavy metal adsorption onto the two adsorbents  $M_1$  and  $M_2$ .

exothermic nature of the adsorption process; besides, its magnitude revealed the type of adsorption mechanism (physisorption or chemisorption). Since the  $\Delta H^\circ$  value was over  $20 \text{ kJ.mol}^{-1}$ , this indicates that the adsorption process of metal ions onto the xerogels occurred by means chemisorption [30]. The observed negative  $\Delta S^\circ$  reflected a lessening in the randomness at the solid/solution interface during the adsorption process [37].

### 4.3 Adsorption mechanism

SEM, FTIR, and XPS analysis have been extensively used to identify the possible metal cation-adsorbent interactions. In order to examine the morphology structure of the adsorbents, SEM micrographs were taken after metal ion adsorption (**Figure 13**).

These micrographs indicated clearly the deformation and the presence of many shiny small particles over the surface of both supports  $M_1$  and  $M_2$  after the adsorption process. Moreover, there was also a decrease in the pore sizes after metal adsorption. This observation evidenced the surface coverage of adsorbents by metal ions.

To gain further insights into the mechanism involved in the metal ions uptake process, the FTIR spectra were analyzed, and the band positions for each adsorbent exposed to metal ions are listed in **Table 8**.

In the  $M_1$  xerogel IR spectrum, the strong band that occurred at around  $3325\text{ cm}^{-1}$  attributed to NH and  $\text{NH}_2$  stretching vibration was shifted and becomes weaker after metal adsorption. This is likely due to the chelation between amino groups and metal ions. Besides, the peak at about  $1614\text{ cm}^{-1}$  ascribed to  $\text{NH}_2$  and NH groups disappeared suggesting that the adsorption process is mainly dominated by the coordination of nitrogen with metal cations. However, the characteristic peak at  $2680\text{ cm}^{-1}$  assigned to the stretching vibration of sulfhydryl group (S-H) was disappeared. This result revealed that metal ions reacted with (S-H) groups on the surface of  $M_2$  xerogel. No obvious shift of the Si-O group after lead adsorption onto the two supports was observed.

To deepen the understanding of the mechanism of metal uptake, XPS analysis before and after metal ion adsorption were performed.

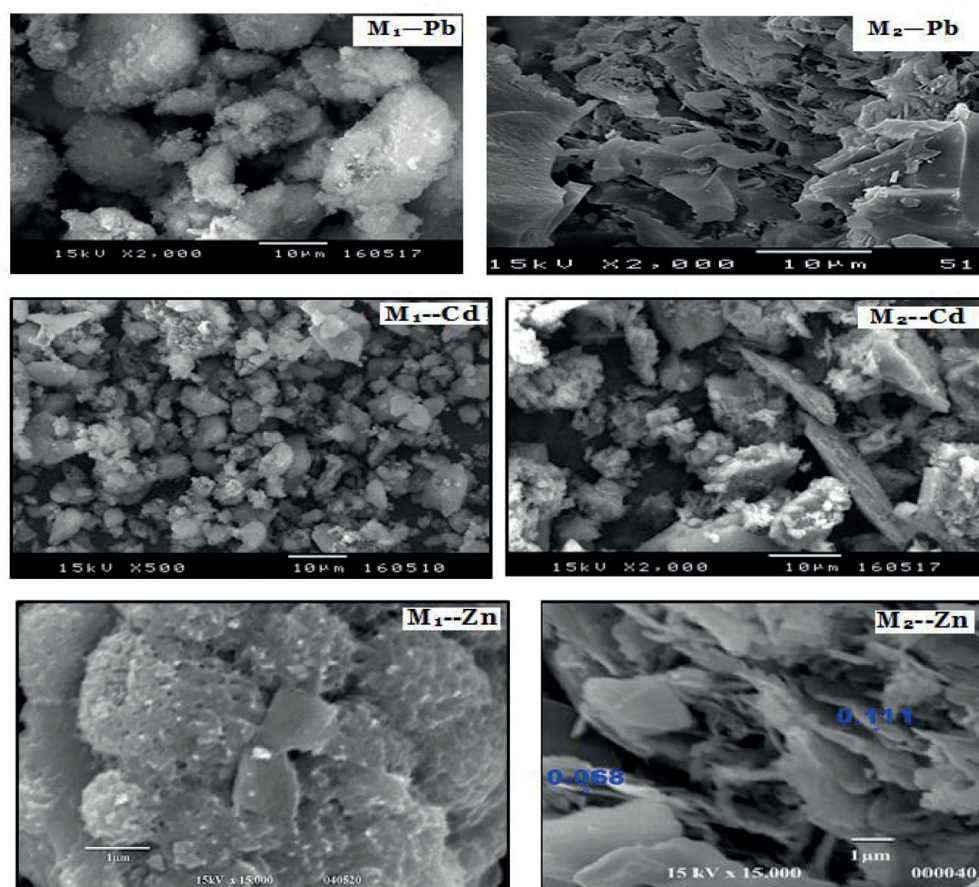


**Figure 13.**  
SEM micrographs of the two adsorbents after metal-ion adsorption.

$\nu$ (cm <sup>-1</sup> )	OH and NH	C=N	Si—N	S—H	Si—O
M <sub>1</sub> (pristine)	3343–3325	1557	1174	—	1058-951-460
Pb <sub>(loaded)</sub>	3303	1559	1170	—	1061-951-464
Cd <sub>(loaded)</sub>	3310	1561	—	—	1060-948-462
Zn <sub>(loaded)</sub>	3307	1558	—	—	1059-950-459
M <sub>2</sub> (pristine)	3383	1576	—	2680	1134-946-434
Pb <sub>(loaded)</sub>	3380	1572	—	—	1131-947-430
Cd <sub>(loaded)</sub>	3383	1574	—	—	1132-949-433
Zn <sub>(loaded)</sub>	3380	1577	—	—	1135-944-436

**Table 8.**  
*Band positions before and after metal cation adsorption.*

As displayed in **Figure 14** a single peak was clearly observed at 398.2 eV, corresponding to the presence of N atom in primary and secondary amine groups. After metal ion adsorption, a new peak with higher binding energy was appeared at about 400.2 eV which may be attributed to the complexation between NH<sub>2</sub> and metal ions (R-NH<sub>2</sub>—M<sup>2+</sup>). On the other hand, the S2p spectra exhibited a faint peak at 167.3 eV assigned to oxidized sulfur. Another peak was observed at 162.6 eV which corresponds to the unbounded S atom in thiol groups. After metal uptake, the peak ascribed to oxidized sulfur becomes much stronger as well as its ratio area, indicating the ion exchange reaction between (S-H) groups on the M<sub>2</sub> xerogel surface and metal ions. Additionally, the XPS spectra of Pb4f, Cd 3d, and Zn2p were also obtained.

As portrayed in **Figure 15**, the binding energies for Pb 4f<sub>7/2</sub>, Cd 3d<sub>5/2</sub>, and Zn2p<sub>3/2</sub> were 137.9 eV, 404.7 eV, and 1021.1 eV, respectively. This result is in agreement with the FTIR analysis which suggests that metal ions form a bidentate complex on amino functionalized xerogel.

5. Performance of the synthesized adsorbents for treatment of electroplating wastewater

The most important part of this work was to evaluate the potential use of both synthesized adsorbents for the treatment of real effluent, via electroplating wastewater. The whole analysis was conducted under the same predetermined conditions (**Figure 16**). The treatment of paint wastewater utilizing hybrid material is represented in **Table 9**.

It is obvious that the adsorption rate decreased from 94%–92% to 78%–76% for M<sub>1</sub> and 92%–92% to 75%–73% for M<sub>2</sub>. This pattern might be clarified by the way that in real discharge, organic matter and other pollutants may rival metal ions leading to lessening removal yield.

5.1 Selectivity of adsorbents

The selectivity of the adsorbent increases its interest for commercial use. In this context, the selectivity of the two xerogels was carried out by removing an aqueous solution containing a mixture of three metal ions (Pb (II), Cd (II), and Zn (II)) under the predetermined optimized conditions, that is, pH = 5, t = 60 min, adsorbent mass = 0.015 g, and T = 20°C.

It is apparent from **Figure 17** that the adsorption efficiency of the two adsorbents towards different ions exposed the following order (Cd<sup>+2</sup> < Pb<sup>+2</sup> < Zn<sup>+2</sup>). The

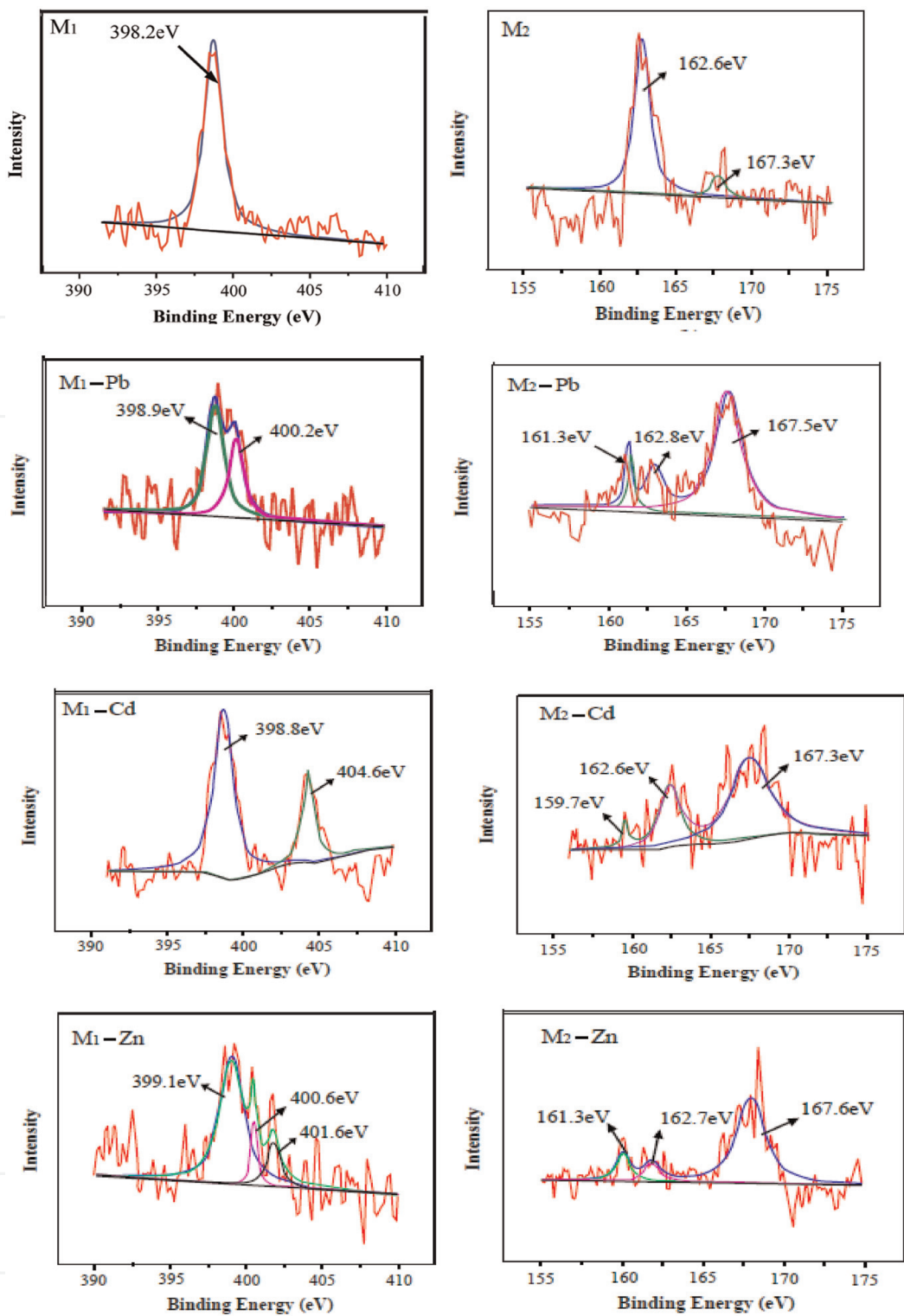


**Figure 14.**  
XPS spectra of N1 s and S2p core level spectra before and after metal cation adsorption.

great selectivity of both xerogels for Zn (II) ions could be ascribed to their low hydrolysis constant and high covalent index. In this regard, the as-prepared adsorbents are relevant for practical application under industrial conditions.

### 5.2 Comparison with different adsorbents

The uptake efficiency of the as-prepared xerogels for the removal of three metal ions (Pb (II), Cd (II), and Zn (II)) was compared with other stated adsorbents (Table 10).



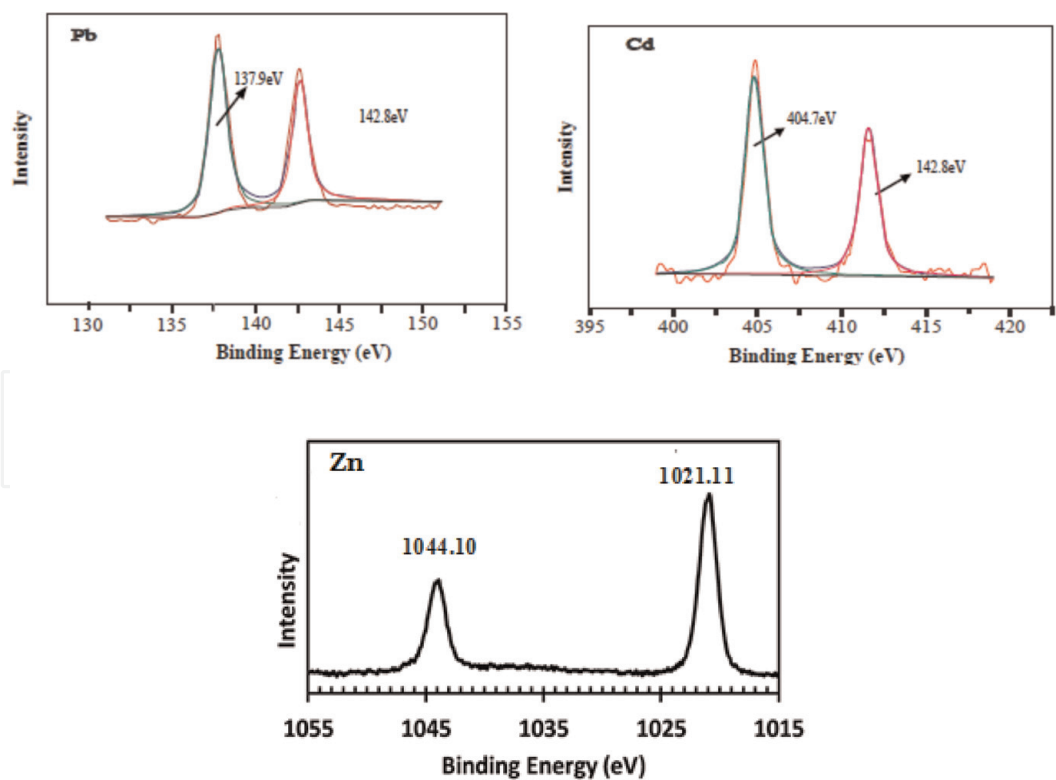


**Figure 15.**  
XPS spectra of Pb4f, Cd 3d, and Zn2p after metal ion adsorption.

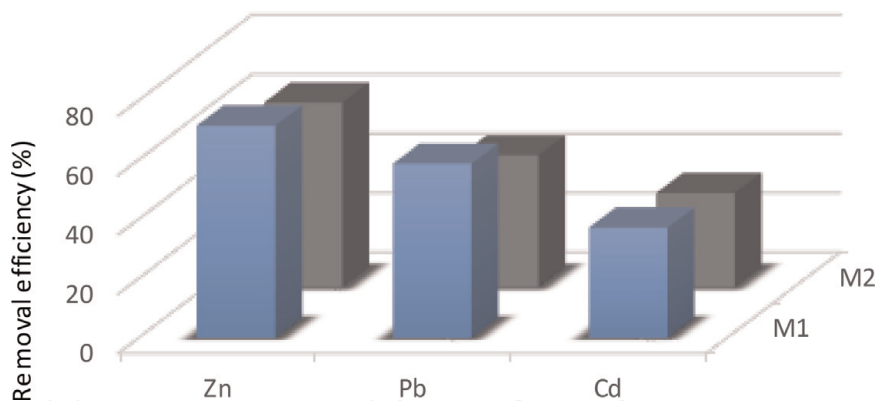


**Figure 16.**  
Efficiency of the as-prepared xerogels for metal ion removal from electroplating wastewater.

Parameters	Values	WHO standard
pH	5.8	5.5–6.5
Temperature	27	20–30
TSS (mg.L <sup>-1</sup> )	419	20
COD (mg.L <sup>-1</sup> )	320	280
BOD (mg.L <sup>-1</sup> )	78	40
Zn (mg.L <sup>-1</sup> )	4.5	5
Pb (mg.L <sup>-1</sup> )	0.15	0.2
Cd (mg.L <sup>-1</sup> )	0.08	0.1

**Table 9.**  
Physicochemical characterization of treated electroplating wastewaters.

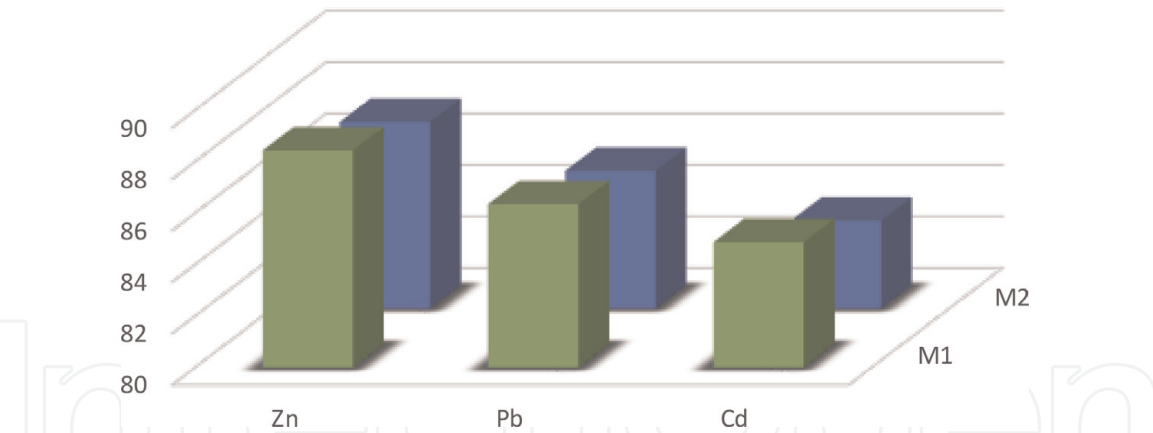


**Figure 17.** Selectivity of **M<sub>1</sub>** and **M<sub>2</sub>** xerogels (adsorbent dosage: 0.4 g. L<sup>-1</sup>; contact time: 60 min; pH: 5; temperature: 20°C).

Adsorbent	pH	Metal ions	q <sub>m</sub> (mg/g)	References
SBA15-NH <sub>2</sub>	5	Pb <sup>2+</sup>	54.6	[38]
PEG-S	6	Pb <sup>2+</sup>	241.36	[39]
Amino xerogel	5	Pb <sup>2+</sup>	523	This work
Sulphydryl xerogel	5	Pb <sup>2+</sup>	509	This work
MIONPs-NH <sub>2</sub>	6	Cd <sup>2+</sup>	33.72	[40]
MC/Al <sub>2</sub> O <sub>3</sub>	3–6	Cd <sup>2+</sup>	49.98	[41]
Amino xerogel	5	Cd <sup>2+</sup>	507	This work
Sulphydryl xerogel	5	Cd <sup>2+</sup>	493	This work
SiNAL4	6	Zn <sup>2+</sup>	86.51	[42]
SG-MCF	6	Zn <sup>2+</sup>	39.96	[43]
Amino xerogel	5	Zn <sup>2+</sup>	578	This work
Sulphydryl xerogel	5	Zn <sup>2+</sup>	549	This work

**Table 10.** Comparison of adsorption capacity of both mesoporous materials **M<sub>1</sub>** and **M<sub>2</sub>** for Pb(II), Cd(II), and Zn (II) with that of other adsorbents.

It can be remarkably noted that the synthesized xerogels exhibited considerably higher adsorption capacity for metal cations than other sorbents specified previously.

This pattern might be attributed to high specific surfaces as well as the number of chelating fragments on the surface of the synthesized adsorbents. Besides, the facility of the synthesis method and the lower adsorption parameters such as contact time, pH solution, and adsorbent dosage made them more appropriate for industrial utilization.

6. Conclusion

The primary targets of this work were to synthesize novel functional organic-inorganic hybrid materials and to check their ability to remove metal ions from aqueous solution. The structural order, morphology, and texture of the prepared

hybrid gels were studied by FTIR,  $^{13}\text{C}$  CP MAS NMR spectroscopy, SEM, and nitrogen adsorption-desorption analysis.

The adsorption kinetic studies abide by the pseudo second-order model and exhibit a three-stage adsorption process. Moreover, the adsorption rate of metal cation was controlled by the diffusion rate inside the pore. The Langmuir model showed the best fit for the entire experimental data. The free energy values ( $E$ ) of metal ion adsorption onto  $\text{M}_1$  and  $\text{M}_2$  xerogels generated by the D-R equation revealed that the adsorption proceeded principally by chemisorption. In column studies, the breakthrough efficiencies of both xerogels were comparable to those calculated from batch techniques and can be reused for at least 5 cycles with a slight decrease in the uptake capacity.

Thermodynamic parameters depicted the spontaneity and the exothermic nature of the adsorption process at 20–40°C. The FTIR and XPS analysis revealed that the chelation between the metal ions and the ligating nitrogen atoms of amino functionalized xerogel was the main mechanism involved in cadmium uptake. Otherwise, the proposed mechanism for lead adsorption onto sulfhydryl xerogel was probably through the ion exchange reaction between metal ions and ( $-\text{SH}$ ) groups. Prior tests accomplished on electroplating wastewater evinced that the xerogel adsorbents possess an exceptional performance in heavy metal uptake from real wastewater. The findings reported in this work showed that the as-prepared xerogels could be widely applied for treatment of industrial wastewater owing to their cost-effectiveness, prominent reusability, good selectivity, and high adsorption efficiency.

## Author details


Yasser Hannachi<sup>1\*</sup>, Afifa Hafidh<sup>2</sup> and Salwa Ayed<sup>1</sup>

<sup>1</sup> Physico-Chemistry Laboratory of Microstructures and Microsystems, IPEST, Tunis, Tunisia

<sup>2</sup> Laboratory of Materials and Environment, Tunis Preparatory Institute for Engineering Studies, Tunis, Tunisia

\*Address all correspondence to: hannachiyasser@gmail.com

## IntechOpen

© 2019 The Author(s). Licensee IntechOpen. This chapter is distributed under the terms of the Creative Commons Attribution License (<http://creativecommons.org/licenses/by/3.0>), which permits unrestricted use, distribution, and reproduction in any medium, provided the original work is properly cited. 

## References

- [1] Manirethan V, Raval K, Rajan R, Thaira H, Balakrishnan MR. Kinetic and thermodynamic studies on the adsorption of heavy metals from aqueous solution by melanin nanopigment obtained from marine source: *Pseudomonas stutzeri*. Journal of Environmental Management. 2018;214:315-324. DOI: 10.1016/j.jenvman. .2018.02.084
- [2] Abdel-Raouf MS, Abdul-Raheim ARM. Removal of heavy metals from industrial waste water by biomass-based materials: A review. Journal of Pollution Effects and Control. 2017;5: 180-193. DOI: 10.4172/2375-4397.1000180
- [3] Chatterjee S, Sivareddy I, De S. Adsorptive removal of potentially toxic metals (cadmium, copper, Nickel and zinc) by chemically treated laterite: Single and multicomponent batch and column study. Journal of Environmental Chemical Engineering. 2017;5: 3273-3289. DOI: 10.1016/j.jece.2017.06.029
- [4] Elkhatab E, Mahdy A, Sherif F, Elshemy W. Competitive adsorption of cadmium (II) from aqueous solutions onto nanoparticles of water treatment residual. Journal of Nanomaterials. 2016;2016:1-10. DOI: 10.1155/2016/8496798
- [5] Torab-Mostaedi M, Asadollahzadeh M, Hemmati A, Khosravi A. Equilibrium, kinetic, and thermodynamic studies for biosorption of cadmium and nickel on grapefruit peel. Journal of the Taiwan Institute of Chemical Engineers. 2013;44:295-302. DOI: 10.1016/j.jtice.2012.11.001
- [6] Hegazi HA. Removal of heavy metals from wastewater using agricultural and industrial wastes as adsorbents. HBRC Journal. 2013;9:276-282. DOI: 10.1016/j.hbrcj.2013.08.004
- [7] Hafidh A, Touati F, Hosni F, Hamzaoui AH, Somrani S. New silica hybrids elaborated by sol-gel process from bifunctional thiadiazole and 1,2,4-triazole precursors. Phosphorus, Sulfur and Silicon and the Related Elements. 2018;193:155-163. DOI: 10.1080/10426507.2017.1393422
- [8] Hafidh A, Touati F, Hamzaoui AH. Synthesis of new silica xerogels based on bifunctional 1,3,4-thiadiazole and 1,2,4-triazole adducts. Journal of Sulfur Chemistry. 2019;40:18-30. DOI: <https://doi.org/10.1080/17415993.2018.1499742>
- [9] Hellali T, Hafidh A, Etteyeb N, Touati F, Hamzaoui AH, Somrani S. New silica-based hybrid materials. Phosphorus, Sulfur and Silicon and the Related Elements. 2017;192:1018-1026. DOI: 10.1080/10426507.2017.1315423
- [10] Paul NE, Diagboya E, Dikio D. Silica-based mesoporous materials; emerging designer adsorbents for aqueous pollutants removal and water treatment. Microporous and Mesoporous Materials. 2018;266: 252-267. DOI: 10.1016/j.micromeso.2018.03.008
- [11] Da'na E. Adsorption of heavy metals on functionalized – Mesoporous silica: A review. Microporous and Mesoporous Materials. 2017;247:145-157. DOI: 10.1016/j.micromeso.2017.03.050
- [12] Kao HM, Chang CH, Saikia D, Liao SH, Chao PY, Chen YH, et al. Highly carboxylic acid functionalized ethane-bridged periodic mesoporous organosilicas: Synthesis, characterization and adsorption properties. Chemistry, an Asian Journal. 2012;7:2111-2117. DOI: 10.1002/asia.201200244
- [13] Vityazev FV, Fedyunova MI, Golovchenko VV, Patova OA, Ipatova EU, Durnev EA, et al. Pectin-silica gels



- as matrices for controlled drug release in gastrointestinal tract. *Carbohydrate Polymers*. 2017;**157**:9-20. DOI: 10.1016/j.carbpol.2016.09.048
- [14] Cristoph S, Fernandes FM, Coradin T. Immobilization of proteins in biopolymer-silica hybrid materials: Functional properties and applications. *Current Organic Chemistry*. 2015;**19**: 1669-1676. DOI: 10.2174/1385272819666150429231937
- [15] Shi J, Tian Y, Liu H, Yang D, Zhang S, Wu Y, et al. Shielding of enzyme by a stable and protective organosilica layer on monolithic scaffolds for continuous bioconversion. *Industrial and Engineering Chemistry Research*. 2017; **56**:10615-10622. DOI: 10.1021/acs.iecr.7b03033
- [16] Santos HA, Makila E, Airaksinen AJ, Bimbo LM, Hirvonen J. Porous silicon nanoparticles for nanomedicine: Preparation and biomedical applications. *Nano*. 2014;**9**:535-534. DOI: 10.2217/nnm.223
- [17] Farghaly AA, Collinson MM. Mesoporous hybrid polypyrrole-silica nanocomposite films with a strata-like structure. *Langmuir*. 2016;**32**:5925-5936. DOI: 10.1021/acs.langmuir.6b00872
- [18] Benhamou A, Baudu M, Derriche Z, Basly JP. Aqueous heavy metals removal on amine-functionalized Si-MCM-41 and Si-MCM-48. *Journal of Hazardous Materials*. 2009;**171**:1001-1008. DOI: 10.1016/j.jhazmat.2009.06.106
- [19] Shahbazi A, Younesi H, Badiei A. Functionalized SBA-15 mesoporous silica by melamine-based dendrimer amines for adsorptive characteristics of Pb(II), Cu(II) and Cd(II) heavy metal ions in batch and fixed bed column. *Chemical Engineering Journal*. 2011;**168**: 505-518. DOI: 10.1016/j.cej.2010.11.053
- [20] Wang W, Tian G, Zhang Z, Wang A. A simple hydrothermal approach to modify palygorskite for high-efficient adsorption of methylene blue and Cu (II) ions. *Chemical Engineering Journal*. 2015;**265**:228-238. DOI: 10.1016/j.cej.2014.11.135
- [21] Adediji JF, Adebayo MA, Ajayi YO, Yusuf LA. Novel mixed ligand of 2,5-diamino-1,3,4-thiadiazole schiff base incorporating benzoic acid: Synthesis and antimicrobial activity. *Journal of Chemical and Pharmaceutical Research*. 2012;**4**:1501-1504
- [22] Ahmed A, Ahmed R, Majed I. Synthesis and characterization of new Schiff bases and using them as tridentate ligands in metal complexes. *International Journal of Applied Science and Technology*. 2014;**4**:108-112
- [23] Rice EW, Baird RB, Eaton AD, Clesceri LS. *Standard Methods for the Examination of Water and Wastewater*. 23rd ed. American Public Health Association. American Water Works Association. Washington DC: Water Environment Federation; 2017
- [24] Xue B, Zhang J, Tang X, Yang C, Chen Q, Man X, et al. Micro-pore structure and gas accumulation characteristics of shale in the Longmaxi formation, Northwest Guizhou. *Petroleum Research*. 2016;**1**:191-204. DOI: 10.1016/s2096-2495(17)30042-x
- [25] Weng CH. Modeling Pb(II) adsorption onto sandy loam soil. *Journal of Colloid and Interface Science*. 2004; **272**:262-270. DOI: 10.1016/j.jcis.2003.11.051
- [26] Rabiul Awual M, Alharthi NH, Okamoto Y, Karim MR, Halim ME, Hasan MM, et al. Ligand field effect for dysprosium(III) and lutetium (III) adsorption and EXAFS coordination with novel composite nanomaterials. *Chemical Engineering Journal*. 2017;**320**: 427-435. DOI: 10.1016/j.cej.2017.03.075

- [27] Lagergren S. Zur theorie der sogenannten, adsorption geloster stoffe, Kungliga Sevenska Ventenskapasa kademiens. The Hand. 1898;**24**:1-39
- [28] Ho YS. Second-order kinetic model for the sorption of cadmium onto tree fern: A comparison of linear and non-linear methods. Water Research. 2006; **40**:119-125. DOI: 10.1016/j.watres.2005.10.040
- [29] Weber WJ, Morris JC. Kinetics of adsorption carbon from solutions. Journal of the Sanitary Engineering Division. 1963;**89**:31-60
- [30] Das B, Mondal NK, Bhaumik R, Roy P. Insight into adsorption equilibrium, kinetics and thermodynamics of lead onto alluvial soil. International journal of Environmental Science and Technology. 2014;**11**:1101-1114. DOI: 10.1007/s13762-013-0279-z
- [31] Langmuir I. The adsorption of gases on plane surface of glass, mica, and platinum. Journal of the American Chemical Society. 1918;**40**:1361-1403. DOI: 10.1021/ja02242a004
- [32] Freundlich H, Helle WJ. Adsorption in solution. Ueber die adsorption in lusungen. Journal of the American Chemical Society. 1939;**61**: 2-28
- [33] Hannachi Y, Rezgui A, Boubaker T. Biosorption potential of the Mediterranean plant (*Posidonia oceanica*) for the removal of Cu<sup>2+</sup> ions from aqueous media: Equilibrium, kinetic, thermodynamic and mechanism analysis. Korean Journal of Chemical Engineering. 2014;**31**:1211-1218. DOI: 10.1007/s11814-014-0054-y
- [34] Dubinin MM, Zaverina ED, Radushkevich LV. Sorption and structure of active carbons. Adsorption of organic vapors. Zhurnal Fizicheskoi Khimii. 1947;**21**:1351-1362
- [35] Kundu S, Gupta AK. Arsenic adsorption onto Iron oxide-coated cement (IOCC): Regression analysis of equilibrium data with several isotherm models and their optimization. Chemical Engineering Journal. 2006; **122**:93-106. DOI: 10.1016/j.cej.2006.06.002
- [36] Hannachi Y, Rezgui A, Dekhil AB, Boubaker T. Removal of cadmium (II) from aqueous solutions by biosorption onto the brown macroalga (*Dictyota dichotoma*). Desalination and Water Treatment. 2015;**54**:1663-1673. DOI: 10.1080/19443994.2014.891078
- [37] Lawal OS, Sanni AR, Ajayi IA, Rabiun OO. Equilibrium, thermodynamic and kinetic studies for the biosorption of aqueous lead (II) ions onto the seed husk of *Calophyllum inophyllum*. Journal of Hazardous Materials. 2010;**177**: 829-835. DOI: 10.1016/j.hazmat.2009.12.108
- [38] Hermàndez-Morales V, Navara R, Acosta-Silva YJ, Macias-Sànchez SA, Pérez-Bueno JJ, Pawelec B. Adsorption of lead (II) on SBA-15 mesoporous molecular sieve functionalized with NH<sub>2</sub> groups. Microporous and Mesoporous Materials. 2012;**160**:133-142. DOI: 10.1016/j.micromeso.2012.05.004
- [39] Tian H, Feng Q, Chen Y, Yang H, Li X, Lu P. Synthesis of amino-functionalized mesoporous materials with environmentally friendly surfactants by evaporation-induced self-assembly and their application to the adsorption of lead(II) ions. Journal of Materials Science. 2015;**50**:2768-2778. DOI: 10.1007/s10853-015-8832-4
- [40] Lin S, Liu L, Yang Y, Lin K. Study on preferential adsorption of cationic-style heavy metals using amine-functionalized magnetic iron oxide nanoparticles (MIONPs-NH<sub>2</sub>) as efficient adsorbents. Applied Surface Science. 2017;**407**:29-35. DOI: 10.1016/j.apsusc.2017.02.173

[41] Yang W, Tang Q, Wei J, Ran Y, Chai L, Wang H. Enhanced removal of Cd (II) and Pb (II) by composites of mesoporous carbon stabilized alumina. *Applied Surface Science*. 2016;**369**: 215-223. DOI: 10.1016/j.apsusc.2016.01.151

[42] Radi S, El Massaoudi M, Bacquet M, Degoutin S, Adarsh NN, Robeyns K, Garcia Y. A novel environment-friendly hybrid material based on a modified silica gel with a bispirazole derivative for the removal of ZnII, PbII, Cd(II) and Cu(II) traces from aqueous solutions. *Inorganic Chemistry Frontiers*. 2017;**4**: 1821-1831. DOI: 10.1039/c7qi00322f

[43] Li M, Li M, Feng C, Zeng Q. Preparation and characterization of multi-carboxyl-functionalized silica gel for removal of Cu (II), Cd (II), Ni (II) and Zn (II) from aqueous solution. *Applied Surface Science*. 2014;**314**: 1063-1069. DOI: 10.1016/j.apsusc.2014.06.038